Far-infrared LMR spectroscopic investigation of the quasi-linear molecule DCCN: The $\nu_5(1 \leftarrow 0)$ transition

W.E. Jones, F. Sun, R.F. Curl, M.D. Allen, K.M. Evenson, and J.M. Brown

Abstract: The far-infrared laser magnetic resonance spectrum (FIR LMR) of the ν_5 bending vibrational transition of DCCN in its $X^3\Sigma^-$ state is reported. The DCCN radical was produced inside the spectrometer cavity by the reaction of deuterated acetonitrile with F atoms. DCCN resonances were measured on seven laser lines. Nitrogen hyperfine structure was observed on a number of the resonances. The analysis provides improved accuracy for the separation $\nu_5 = 1 \leftarrow 0$ and some of the ^{14}N hyperfine coupling constants for this isotopomer.

PACS No.: 33.20Ea

Résumé: Nous présentons le spectre de résonance magnétique laser dans l'infrarouge lointain (FIR LMR) de la transition de vibration de flexion ν_5 du DCCN dans son état $X^3\Sigma^-$. Le radical DCCN est produit dans l'enceinte du spectromètre par la réaction entre de l'acétonitrile deutérée et des atomes de F. Nous avons mesuré des résonances du DCCN sur sept lignes lasers. Nous avons observé la structure hyperfine de l'azote sur plusieurs résonances. Cette étude améliore la précision dans les mesures de la séparation $\nu_5 = 1 \leftarrow 0$ et de quelques constantes du couplage hyperfin de ^{14}N dans cet isotopomère.

[Traduit par la rédaction]

1. Introduction

Since the first observation of the ESR spectrum of HCCN in 1964 [1], the radicals HCCN and DCCN have attracted considerable attention both experimentally and theoretically. The stimulus for

Received June 19, 2000. Accepted September 8, 2000. Published on the NRC Research Press Web site on March 7, 2001.

W.E. Jones.[1] School of Physical Sciences, University of Windsor, Windsor, ON N9B 3P4, Canada.
F. Sun and R.F. Curl. Department of Chemistry and Rice Quantum Institute, Rice University, Houston, TX 77005, U.S.A.
M.D. Allen and K.M. Evenson. National Institute of Standards and Technology, Time and Frequency Division 847, 325 Broadway, Boulder, CO 80303, U.S.A.
J.M. Brown. Physical and Theoretical Chemistry Laboratory, South Parks Road, Oxford, OX1 3QZ, United Kingdom

[1] Corresponding author Department of Chemistry and Biochemistry, School of Physical Sciences, University of Windsor, 401 Sunset Ave., Windsor, ON N9B 3P4, Canada. Telephone: (519) 253-3000-2684; FAX: (519) 973-7098; e-mail: wjones@uwindsor.ca

 DOI: 10.1139/cjp-79-2/3-389

this interest has been primarily to answer the question whether these radicals are linear or bent, and much labor has focused on the characterization of the HCC bending potential.

Early matrix isolation EPR [1–4], infrared [5], and microwave spectra [6] of HCCN provided evidence to suggest the radical was linear in a triplet electronic state. The microwave spectrum reported by Saito et al. [6] showed an apparent absence of K-type satellite transitions, and their observed transition frequencies closely fit a simple linear molecule Hamiltonian including the effects of electron and nuclear spin.

The linear configuration for HCCN suggested by the early experimental studies was not supported by later ab initio calculations [7–10]. Kim et al. [7] predicted that a bent structure for HCCN was about 2 kcal mol^{-1} more stable than the linear configuration. They argued that the barrier between bent and linear configurations was so small that thermal motions yielded a linear vibrationally averaged structure, which they described as "quasi-linear." Subsequent calculations (8)–(10) showed greater stability of the bent structure of HCCN, but the barrier to linearity has decreased with higher levels of theory and larger basis sets. In the most elaborate calculation done in 1992, Seidl and Schaefer [10] estimated the HCC angle of the minimum energy configuration to be 142.3° and the barrier to linearity as 0.79 kcal mol^{-1} (277 cm^{-1}).

In 1990, Brown et al. [11], from measurements of the microwave spectrum of isotopically substituted HCCN, reported the r_s structure as, $r_{(C-H)} = 0.998$, $r_{(C-C)} = 1.323$, and $r_{(C-N)} = 1.195$ Å. They concluded that the abnormally short C–H bond length could be explained as an average over the large amplitude of the HCC bending expected for a quasi-linear molecule.

It thus appears from both theoretical and experimental results that HCCN and its isotopomers are quasi-linear. In referring to the various vibrational modes of DCCN, it is convenient to designate these modes as though the molecule were linear; thus ν_1 for CD stretching, ν_2 for CCN (roughly) out of phase stretching, ν_3 for CCN (roughly) in phase stretching, ν_4 for CCN bending and finally ν_5 for CCD bending. To determine the HCC (DCC) bending angle and understand its bending potential, energy levels associated with the HCC (DCC) bending must be obtained and a number of spectroscopic investigations [12–16] have focused on transitions involving the ν_5 bending mode. A high-resolution study of the ν_1 CH stretching fundamental by Morter et al. [12] estimated the vibrational energy of ν_5 for HCCN at 187 ± 20 cm^{-1} by comparing the relative intensities of ν_1 and $\nu_1 + \nu_5 - \nu_5$ transitions. McCarthy et al. [14] re-examined the microwave spectra of HCCN and DCCN and found several vibrational satellites involving ν_4 and ν_5. For HCCN, McCarthy et al. [14] observed the ground state, ν_5, $2\nu_5^{\pm 2}$, $3\nu_5^{\pm 3}$, ν_4, and three $l = 0$ states. Three $l = 0$ states are expected, one corresponding to $2\nu_5{}^0$, and a pair corresponding to the two ways that a $(\nu_4 + \nu_5)^0$ state can be created. However, it is not known which, if any, of the three states corresponds to $2\nu_5{}^0$. For DCCN, McCarthy et al. [14] observed the ground state, ν_5, $2\nu_5^{\pm 2}$, $3\nu_5^{\pm 3}$, ν_4 but only one $l = 0$ state. In recent studies of the $\nu_1 + \nu_5$ combination and hot bands, the energy of the lowest excited state with angular momentum about the A-axis, ν_5, was determined to be 128.907 cm^{-1} for HCCN [15] and 74.845 cm^{-1} for DCCN [16], both somewhat less than the energies predicted by McCarthy et al. [14], namely, 145 ± 15 cm^{-1} and 90 ± 15 cm^{-1} for HCCN and DCCN, respectively.

In this paper we report the far-infrared laser magnetic resonance observation of the ν_5 bending vibrational transition of DCCN in its $\boldsymbol{X}\ ^3\Sigma^-$ state. These measurements were made on the far-infrared laser magnetic resonance (FIR LMR) instrument at the National Institute of Standards and Technology, Time and Frequency Division 847, Boulder, CO. The ground and ν_5 states were effectively treated in isolation. In order to obtain the best parameters, the data set, which was used, contained the microwave measurements of Brown et al. [11] and of McCarthy et al. [14] as well as the LMR results of this work. Nitrogen hyperfine structure was observed on a number of LMR lines; splitting due to (^{2}H) deuterium hyperfine structure was not observed. The LMR data taken in this work improve the accuracy of the separation $\nu_5 = 1 \leftarrow 0$, and provides hyperfine coupling constants for this isotopomer.

Fig. 1. Sample far-infrared survey trace on the 2188.9290 GHz (136.959 μm) laser line of CD_3OD pumped by the 9P(26) line of CO_2. The spectrum was recorded in parallel polarization ($\Delta M_J = 0$), centered at 1000 mT with a span of 200 mT, modulation 0.5 of maximum, time constant 300 ms, scan time 5 min, sensitivity 500 μV. Four typical resonances are shown.

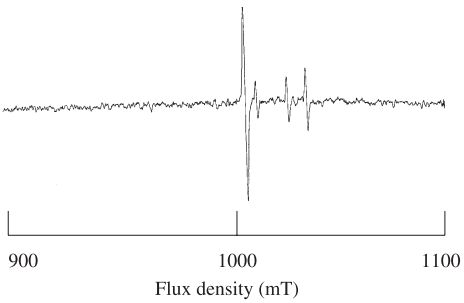

Fig. 2. Sample measurement trace on the 2314.1113 GHz (129.550 μm) laser line of CH_3OH pumped by the 10R(34) line of CO_2, showing the resonance at 1773.21 mT. The spectrum was recorded in perpendicular polarization ($\Delta M_J = \pm 1$), centered at 1776 mT with a span of 20 mT. (A), $P_{tot} = 250$ mTorr, modulation 0.5 of maximum, time constant 1 s, scan time 5 min, sensitivity 1.0 mV. (B), $P_{tot} = 250$ mTorr, modulation 0.1, time constant 1 s, scan time 5 min, sensitivity 200 μV.

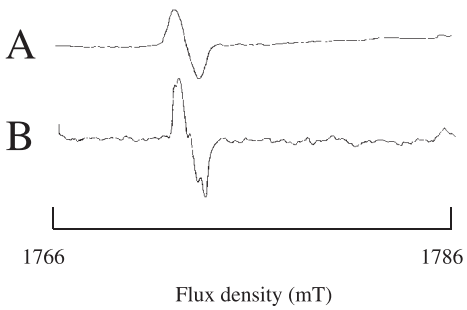

Fig. 3. Traces showing development of hyperfine structure of the resonances near 1125 mT. The traces were taken with the 2252.0542 GHz (133.120 μm) laser line of CH_3OH pumped by the 9P(24) CO_2 laser line in parallel polarization. The traces are centered at 1.125 T, with a width of 0.02 T under the conditions: $P_{tot} = 200$ mTorr, scan rate 10 min, and time constant 1 s; (A), 1 mV and modulation 0.5 of maximum; (B), 1 mV and modulation 0.2 of maximum; and (C) at 500 μV and modulation 0.1 of maximum.

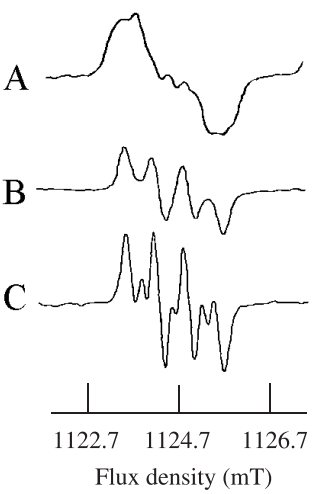

Fig. 4. Two resonances, assigned as $N = 2$, $M_J = 0$, $Id\sharp = 1 \leftarrow N = 2$, $M_J = 0$, $Id\sharp = 3$; and $N = 2$, $MJ = 1$, $Id\sharp = 1 \leftarrow N = 2$, $M_J = 1$, $Id\sharp = 3$ observed over three laser lines. The laser lines are (A), 2217.899 GHz (135.173 μm) of CH_2DOH pumped by the 10R(32) line of CO_2. (B), 2216.2635 GHz (135.269 μm) of CH_2F_2 pumped by the 9P(24) line of CO_2. (C), 2207.0583 GHz (135.834 μm) of CH_2DOH pumped by the 9R(08) line of CO_2.

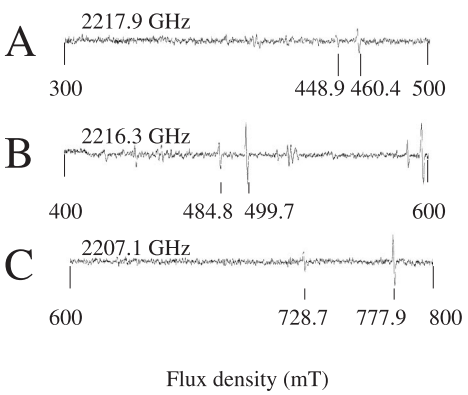

2. Experimental

DCCN was produced by fluorine atom extraction of deuterium from deuterated acetonitrile (CD_3CN, 99.8% purity from Cambridge Isotopes Laboratory). This method has proven effective in previous studies

Fig. 5. Chart of tuning curves from 2140 to 2340 GHz including the transitions observed in the present work. Continuous lines indicate positions of the seven laser lines used. The regions, where the same two transitions cross three laser lines, are indicated by arrows. Only those regions of the tuning curves where the intensity of a resonance would be $\geq$25 are shown as a continuous curve.

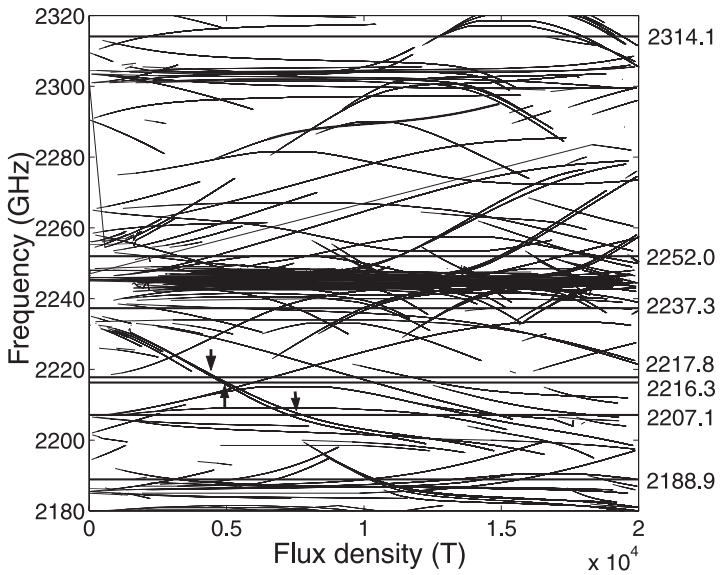

Fig. 6. Two regions taken in perpendicular polarization with the 2252.0542 GHz (133.120 μm) laser line illustrating many overlapped and broad transitions that resulted in inaccurate measurements of the DCCN resonances on this line between 0 and 400 mT. The upper curve (A), covers the region 190.0 to 210.0 mT. The lower curve (B) shows the region 224.6 to 244.6 mT.

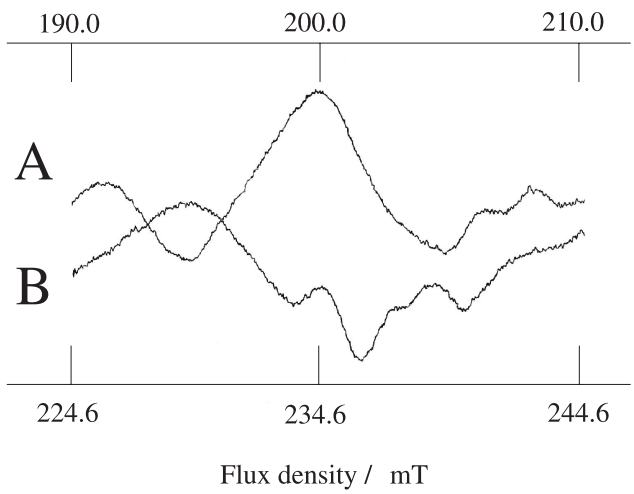

[17] and has been used recently for the production of HCCN from CH_3CN[2] for an LMR study of the radical HCCN. A microwave discharge produced fluorine atoms in a flowing mixture of 10% F_2 in He. The deuterated acetonitrile was added downstream directly in the laser cavity where a deep purple flame was observed indicating optimization of the production of DCCN by the removal of two D atoms

[2] M.D. Allen, K.M. Evenson, and J.M. Brown. Manuscript in preparation.

Table 1. Laser lines used in the FIR–LMR study of DCCN.

CO_2 pump	Lasing medium	Wavelength (μm)	Frequency (GHz)	Wave number (cm^{-1})	DCCN transitions observed	
10R(34)	CH_3OH	129.550	2314.1113	77.190 446	$\Delta N = 0$;	$N'' = 3$
					$\Delta N = +1$;	$N'' = 2, 3$
9P(24)	CH_3OH	133.120	2252.0542	75.120 444	$\Delta N = -1$;	$N'' = 2$
					$\Delta N = 0$;	$N'' = 1, 2, 3, 4, 5, 6$
					$\Delta N = +1$;	$N'' = 0, 1, 2, 3$
9P(22)	CH_2F_2	133.998	2237.3964*	74.631 512	$\Delta N = -1$;	$N'' = 2, 3, 4, 5$
					$\Delta N = 0$;	$N'' = 1, 2, 3, 5$
					$\Delta N = +1$;	$N'' = 1$
10R(32)	CH_2DOH	135.173	2217.8499	73.979 511	$\Delta N = 0$;	$N'' = 2$
9P(24)	CH_2F_2	135.269	2216.2635	73.926 594	$\Delta N = 0$;	$N'' = 2$
9R(08)	CH_2DOH	135.834	2207.0583	73.619 542	$\Delta N = 0$;	$N'' = 2$
10R(46)	CD_3OD	136.959	2188.9290	73.014 814	$\Delta N = -1$;	$N'' = 3$
					$\Delta N = 0$;	$N'' = 3$

* Line frequency corrected from that reported by Douglas [20].

by F. Optimum signals were obtained with partial pressures of approximately 335 and 40 mTorr for the mixture of 10 %F_2 / 90 %He and CD_3CN, respectively. Two checks, one using CH_3CN and one using CH_4 as reactant, were performed on most of the transitions to confirm that the signals were due to DCCN. On occasion, CD_4 or CD_3OD was used to confirm that the signals were not from CD or oxygen containing species.

The far-infrared laser magnetic resonance spectrometer used is very similar to that described in detail by Saykally et al. [18]. The sensitivity and short-wavelength performance of this spectrometer were recently improved by two modifications to the apparatus [19]. The Zeeman modulation frequency was increased from 13 to 40 kHz with subsequent increase in the sensitivity. A reduction in the diameter (from 50.4 to 19 mm) of the tube comprising the pump region, giving greater overlap of the FIR radiation field at short wavelengths with the pumped lasing gas, provided an increase of the power of FIR laser lines with wavelengths less than 100 μm.

Resonance signals, detected with a germanium (Ge) bolometer cooled to 1.5 K, were processed by a lock-in amplifier at $1f$, and recorded with a xy plotter as a function of flux density. Since $1f$ detection using magnetic modulation was employed, the first derivative of the absorption peak was observed.

The magnet was calibrated with a NMR gaussmeter. The overall experimental uncertainty is estimated to be $((\pm 1 \times 10^{-4}) \times B$ (T)) above 0.1 T and $\pm 1 \times 10^{-5}$ below 0.1 T, where B is the magnetic flux density. The laser frequency as used in the experiment is accurate to $(2^{1/2} \times (2 \times 10^{-7}) \times \nu_{\text{laser}})$.

3. Results

Survey and measurement spectra were taken with the electric field of the laser in both parallel ($E\omega \,||\, B_0$) and perpendicular ($E\omega \perp B_0$) polarization to the magnetic field. A sample survey spectrum is shown in Fig. 1. This figure presents a 200 mT portion (center at 1 T) of the DCCN spectrum observed on the 2 188.9290 GHz (136.959 μm) laser line taken in parallel polarization ($\Delta M_J = 0$). For the most part, the DCCN lines were quite weak. Measurement scans were typically $\leq$20 mT in width, as shown in Fig. 2, where the perpendicular line at 1773.21 mT is shown. The upper trace (A) was taken using a sensitivity of 1.0 mV and a modulation of 0.5 of maximum, while trace B shows Lamb-dips due to the ^{14}N hyperfine splitting and was taken with sensitivity of 200 μV sensitivity and a modulation of 0.1 of maximum. The resonances were measured by tuning the magnet to the center of the line and waiting several time constants for the magnetic field to stabilize.

Table 2. Conversion relationships between linear and bent molecules.

Linear notation	Bent notation
ν_0 of ν_5	$\left(A - \frac{1}{2}(B+C)\right)$
B_0	$\frac{1}{2}(B+C)$
D_0	Δ_N
γ_0	$\frac{1}{2}(\epsilon_{\rm bb} + \epsilon_{\rm cc})$
λ_0	$3\alpha/2$
λ_{D0}	$3\Delta_N^\alpha/2$
B_1	$\frac{1}{2}(B+C) - D_{NK}$
D_1	$D_{\rm N} - \Phi_{NK}$
γ_1	$\frac{1}{2}(\epsilon_{\rm bb} + \epsilon_{\rm cc}) + (\Delta_{NK}^{\rm S} + \Delta_{KN}^{\rm S})$
λ_1	$3\alpha/2 + 3\Delta_K^\alpha/2$
λ_{D1}	$3\Delta_N^\alpha/2 + 3\Phi_{NK}^\alpha/2$
o	β
p	$-\frac{1}{2}(\epsilon_{\rm bb} - \epsilon_{\rm cc})$
q	$\frac{1}{2}(B-C)$
q_D	$-2\delta_N$
b_F (N)	a_F (N)
c (N)	$3aa_I/2$ (N)
d	$[(bb)_I - (cc)_I]$ (N)
eQq (N)	$aa_Q(2I(2I-1))$ (N)

Fifteen lines showed hyperfine splitting arising from the nuclear spin of the ^{14}N ($I = 1$) nuclei. The hyperfine structure was resolved by significantly reducing the pressure and modulation amplitude in order to resolve the Lamb-dips. A sample showing the expected triplet hyperfine structure is given in Fig. 3 (trace B), which shows the parallel resonance at 1123.65 mT, taken with the 2252.0542 GHz (133.120 μm) laser line of CH_3OH pumped by the 9P(24) line of CO_2. Trace C in this figure shows clearly the Lamb dips in the hyperfine structure for ^{14}N ($I_{\rm N} = 1$). The spectrum appears somewhat more complicated than expected for the $3M_{\rm F}$ components of ^{14}N hyperfine splitting but not sufficiently resolved to be convincing evidence of deuterium splitting.

We were able to identify two resonances which occurred over three laser lines 2207.0583 GHz (135.834 μm), 2216.2635 GHz (135.269 μm), and 2217.8499 GHz, (135.173 μm) as shown in Fig. 4. The positioning of these six resonances is shown in Fig. 5. This figure presents the transition frequencies in magnetic fields from 0 to 2 T over the frequency range 2140 to 2340 GHz for DCCN. The positions of each of the seven laser lines used in this work are shown as continuous horizontal lines. Arrows in Fig. 5 depict the positions of the six resonances observed on the three laser lines.

A region of extremely broad resonances occurred between 190.0 and 210.0 mT on the 2252.0542 GHz (133.120 μm) laser line in perpendicular polarization. These broad resonances resulted in inaccurate measurements on a number of lines identified in Table 3. An example of the region is shown in Fig. 6.

Table 1 provides details on the seven laser lines used to record the LMR spectra reported in this paper. This table also provides a summary of the DCCN transitions observed on each line.

In all, 157 transitions were observed which belong to the $\nu_5 = 1 \leftarrow 0$ transition. Of these, 15 were found to have large uncertainties, either because of overlapping resonances, extremely weak character, or exceedingly poor line shape, and were not used in the fit. As mentioned previously, examples of the problem of broad and/or underlying resonances are shown in Fig. 6. Fifteen resonances showed well-developed N hyperfine structure.

Table 3. Details of the observed FIR–LMR resonances and the least-squares fit for DCCN in the $\nu_5 = 0 \leftarrow 1$ transition.

N	M_J	$Id\sharp^{\prime}$	M_I (^{14}N)	Field (mT)	Tuning rate (MHz/mT)	Intensity (arb. units)	Obs.–calc. (MHz)	Assigned uncertainty (MHz)
Laser frequency 2188.9290 GHz (136.959 μm)								
2 ← 3	0 ← 0	2 ← 1		162.44	10.5	48.0	1.3	2
2 ← 3	3 ← 3	1 ← 1		310.69	16.0	32.9	1.5	2
2 ← 3	−2 ← −2	2 ← 2		316.69	−8.6	62.7	−0.3	2
2 ← 3	1 ← 1	1 ← 1		525.17	10.6	47.4	1.5	2
2 ← 3	0 ←0	1 ← 1		679.28	21.0	58.5	−1.7	2
2 ← 3	0 ← 0	2 ← 2		1014.69	7.4	92.8	−0.4	2
3 ← 3	0 ← 0	1 ← 3		1019.51	−35.9	41.4	0.8	2
3 ← 3	2 ←2	1 ← 3		1032.79	−30.0	49.7	−1.1	2
3 ← 3	1 ← 1	1 ← 3		1040.78	−29.0	62.1	−2.3	2
2 ← 3	2 ← 2	1 ←2		1332.49	6.3	61.4	1.0	6
2 ← 3	1 ← 1	2 ← 2		1438.07	12.5	49.0	−0.7	2
2 ← 3	−1 ← −1	1 ← 1		1570.97	13.9	62.4	0.3	2
2 ← 3	0 ← 1	1 ← 1		606.60	13.1	90.4	1.3	2
2 ← 3	0 ← −1	1 ← 1		680.04	21.3	27.9	−0.4	2
3 ← 3	1 ← 0	1 ← 3		1049.72	−27.9	39.4	1.3	2
3 ← 3	0 ← −1	1 ← 3		1056.52	−30.4	59.3	2.7	4
3 ← 3	−1 ← −2	1 ← 3		1061.47	−37.6	61.2	13.1	0*
3 ← 3	1 ← 2	1 ← 3		1067.60	−25.4	42.1	−1.6	2
3 ← 3	2 ← 3	1 ← 2		1113.56	−20.0	91.5	−0.6	2
2 ← 3	0 ← −1	2 ← 2		1116.63	10.3	46.9	−1.5	4
2 ← 3	0 ← 1	2 ← 2		1151.84	11.4	44.3	−2.3	6
2 ← 3	1 ← 0	2 ← 2		1300.37	6.4	30.7	−0.1	2
Laser frequency 2207.0583 GHz (135.834 μm)								
2 ←2	0 ← 0	1 ← 3		728.74	−28.3	36.6	0.0	2
2 ← 2	1 ← 1	1 ← 3		777.90	−24.5	59.8	−3.2	2
Laser frequency 2216.2635 GHz (135.269 μm)								
2 ← 2	0 ← 0	1 ← 3		484.79	−43.8	26.9	−8.1	6
2 ← 2	1 ← 1	1 ← 3		499.68	−39.9	51.6	−5.8	6
Laser frequency 2217.8499 GHz (135.173 μm)								
2 ← 2	0 ← 0	1 ← 3		448.91	−44.3	27.1	−2.4	4
2 ← 2	1 ← 1	1 ← 3		460.40	−40.9	52.3	−6.4	4
Laser frequency 2237.3964 GHz (133.998 μm)								
1 ← 1	0 ← 0	1 ← 2		222.50	−11.6	78.7	−1.7	2
1 ← 2	0 ← 0	3 ← 1		689.20	27.9	107.3	4.2	2
1 ← 1	0 ← 0	3 ← 3		749.62	−30.9	96.7	4.9	2
2 ← 3	2 ← 2	2 ← 1		999.64	32.9	139.1	−0.1	2

Table 3. (*continued.*)

N	M_J	$Id\sharp^{\iota}$	M_I (^{14}N)	Field (mT)	Tuning rate (MHz/mT)	Intensity (arb. units)	Obs.–calc. (MHz)	Assigned uncertainty (MHz)
Laser frequency 2237.3964 GHz (133.998 μm) continued								
2 ← 3	1 ← 1	3 ← 1		1 024.31	29.8	77.2	5.1	6
2 ← 2	2 ← 2	2 ← 2		1 055.76	−25.7	68.7	−6.5	6
2 ← 2	0 ← 0	3 ← 3		1 087.01	−31.5	48.1	−0.1	2
3 ← 4	3 ← 3	2 ← 1		1 318.03	41.7	98.3	−1.2	2
2 ← 1	0 ← 0	1 ← 3		1 442.05	−20.3	69.2	2.2	2
3 ← 3	3← 3	2 ← 2		1 476.94	−40.4	56.5	11.7	0*
2 ← 3	0 ← 0	2 ← 1		1 631.25	45.2	49.0	8.0	6
4 ← 5	3 ← 3	3 ← 1		1 662.41	44.8	55.7	1.1	2
1 ← 1	1 ← 2	1 ← 1		84.96	−19.0	102.2	−1.5	2
2 ← 2	−2 ← –1	2 ← 3		182.34	−14.4	67.1	−2.4	2
5 ← 5	−4 ← –5	2 ← 2		269.42	11.9	78.1	−2.2	4
1 ← 1	0 ← −1	2 ← 2		272.92	11.7	121.7	0.1	2
2 ← 2	0 ← 1	1 ← 2		410.03	−22.0	60.2	0.7	2
2 ← 2	−1 ← 0	1 ← 2		429.62	−24.6	45.8	−1.6	2
1 ← 1	0 ← 1	3 ← 2		619.41	−18.3	183.9	0.9	2
1 ← 2	0 ← −1	3 ← 1		686.97	28.8	135.4	−2.6	2
1 ← 2	1 ← 0	2 ← 1		970.18	13.8	145.8	−2.7	2
2 ← 3	0 ← −1	3 ← 1		1 016.42	35.9	113.7	−5.6	2
2 ← 2	1 ← 0	3 ← 3		1 039.58	−26.4	155.5	−0.6	2
2 ← 3	2 ← 1	2 ← 1		1 042.88	30.0	94.0	−3.0	2
2 ← 3	1 ← 0	3 ← 1		1 054.66	27.5	143.8	−3.1	2
2 ← 2	0 ← 1	3 ← 3		1 066.24	−27.9	159.1	−1.4	2
2 ← 2	1 ← 2	3 ← 2		1 075.33	−30.1	124.7	−2.1	4
2 ← 2	0 ← −1	1 ← 2		1 120.95	13.4	146.4	−1.4	2
2 ← 1	0 ← 1	1 ← 2		1 282.82	−15.0	96.3	−0.7	2
1 ← 1	0 ← −1	2 ← 2		1 339.17	−14.0	83.2	−1.4	4
3 ← 4	1 ← 0	3 ← 1		1 347.64	38.1	95.2	1.5	2
3 ← 4	2 ← 1	3 ← 1		1 356.22	35.5	88.5	2.4	2
1 ← 2	0 ← −1	2 ← 1		1 362.70	12.8	179.9	−3.4	2
3 ← 3	3 ← 2	2 ← 3		1 416.63	−31.7	104.5	2.2	2
3 ← 3	2 ← 1	3 ← 3		1 419.23	−33.9	120.5	−1.2	4
3 ← 3	1 ← 0	3 ← 3		1 454.81	−39.3	90.3	1.0	2
3 ← 3	0 ← 1	3 ← 3		1 472.66	−41.9	76.6	4.8	2
2 ← 2	1 ← 2	1 ← 1		1 475.85	6.8	193.3	0.7	4
3 ← 3	−1 ← 0	3 ← 3		1 490.70	−45.7	46.5	6.7	6
1 ← 2	−1 ← –2	2 ← 1		1 505.55	15.3	171.9	−2.6	2

Table 3. (*continued.*)

N	M_J	$Id\sharp^{\iota}$	M_I (^{14}N)	Field (mT)	Tuning rate (MHz/mT)	Intensity (arb. units)	Obs.–calc. (MHz)	Assigned uncertainty (MHz)
Laser frequency 2237.3964 GHz (133.998 μm) concluded								
1 ← 1	1 ← 2	2 ← 1	1 ← 1	727.94	−24.8	201.7	1.5	2
1 ← 1	1 ← 2	2 ← 1	0 ← 0	728.54	−24.8	201.7	3.1	2
1 ← 1	1 ← 2	2 ← 1	−1 ← −1	729.04	−24.8	201.7	2.4	2
2 ← 2	2 ← 1	3 ← 6	1 ← 1	981.37	−17.4	205.9	−1.2	2
2 ← 2	2 ← 1	5 ← 8	0 ← 0	981.87	−17.4	206.0	0.6	2
2 ← 2	2 ← 1	6 ← 8	−1 ← −1	982.37	−17.4	206.1	0.9	2
3 ← 3	1 ← 2	3 ← 3	1 ← 1	1469.96	−41.0	74.7	−2.2	2
3 ← 3	1 ← 2	8 ← 7	0 ← 0	1470.26	−41.0	74.8	−4.5	2
3 ← 3	1 ← 2	7 ← 7	−1 ← −1	1470.66	−41.0	74.7	−3.3	2
Laser frequency 2252.0542 GHz (133.120 μm)								
1 ← 1	0 ← 0	1 ← 1		207.14	−9.1	340.6	0.9	2
1 ← 1	−1 ← −1	2 ← 1		453.61	20.8	78.9	−1.1	2
1 ← 1	1← 1	2 ← 1		602.82	6.9	42.2	−0.2	2
2 ← 1	0 ← 0	1 ← 3		607.22	−35.3	109.1	−0.2	2
1 ← 0	0 ← 1	2 ← 1		639.67	−18.7	71.5	−1.3	2
2 ← 1	−1 ← −1	1 ← 2		1062.85	−23.0	43.9	1.6	2
3 ← 3	0 ← 0	1 ← 1		1179.55	40.1	14.2	5.8	6
2 ← 1	0 ← 0	2 ← 3		1184.39	−13.2	186.2	−5.0	4
4 ← 3	3 ← 3	1 ← 2		1265.26	−44.3	42.5	1.6	2
4 ← 4	2 ← 2	1 ← 1		1493.89	38.6	98.2	−5.0	2
2 ← 1	0 ← 0	3 ← 3		1686.30	−40.9	94.6	8.4	4
1 ← 2	0 ← 0	3 ← 1		1724.29	19.6	111.0	−2.3	2
5 ← 5	3 ← 3	1 ← 1		1866.03	42.3	86.8	−27.1	0*
5 ← 5	4 ← 4	1 ← 1		1884.94	43.5	112.7	7.0	8
1 ← 1	−1 ← 0	1 ← 1		98.45	−12.5	356.3	−2.8	2
3 ← 3	3 ← 4	2 ← 1		145.74	−15.0	56.9	12.4	0∋
1 ← 0	0 ← 1	1 ← 1		180.64	−41.4	124.7	3.0	2
2 ← 2	0 ← 1	2 ← 1		204.93	15.3	118.0	−17.7	0∋
3 ← 3	–3 ← −2	2 ← 2		207.23	−12.9	127.2	13.9	0∋
2 ← 2	−1 ← 0	2 ← 1		233.93	14.0	127.8	−0.3	2
4 ← 4	−4 ← −3	2 ← 2		237.93	−14.0	86.4	15.1	0∋
5 ← 5	−5 ← −4	2 ← 2		261.02	−14.7	64.0	16.5	0∋
1 ← 1	0 ← −1	2 ← 1		270.62	25.7	125.4	−10.8	0∋
1 ← 1	1 ← 0	2 ← 2		273.61	25.2	134.0	−5.6	6
6 ← 6	6 ← 7	2 ← 1		277.61	−15.0	37.5	−28.0	0∋
1 ← 1	2 ← 1	1 ← 1		332.08	20.9	113.5	−7.2	8

Table 3. (*continued.*)

N	M_J	$Id\sharp^{t}$	M_I (^{14}N)	Field (mT)	Tuning rate (MHz/mT)	Intensity (arb. units)	Obs.–calc. (MHz)	Assigned uncertainty (MHz)
Laser frequency 2252.0542 GHz (133.120 μm) continued								
$1 \leftarrow 0$	$-1 \leftarrow 0$	$1 \leftarrow 1$		338.78	−23.1	64.6	−1.3	2
$2 \leftarrow 2$	$3 \leftarrow 2$	$1 \leftarrow 1$		438.12	21.0	69.3	6.3	10
$1 \leftarrow 1$	$0 \leftarrow -1$	$3 \leftarrow 2$		444.81	17.8	138.9	−0.4	2
$2 \leftarrow 2$	$1 \leftarrow 0$	$1 \leftarrow 1$		748.63	25.3	107.3	2.7	2
$2 \leftarrow 2$	$0 \leftarrow -1$	$1 \leftarrow 1$		810.27	32.1	105.5	1.3	2
$3 \leftarrow 2$	$2 \leftarrow 1$	$1 \leftarrow 3$		878.89	−42.8	70.8	1.9	2
$3 \leftarrow 2$	$1 \leftarrow 0$	$1 \leftarrow 3$		923.94	−39.9	95.9	2.5	2
$3 \leftarrow 2$	$1 \leftarrow 2$	$1 \leftarrow 2$		946.91	−36.8	99.5	−1.3	2
$1 \leftarrow 1$	$0 \leftarrow -1$	$3 \leftarrow 2$		980.17	−17.0	144.2	3.7	2
$2 \leftarrow 1$	$0 \leftarrow 1$	$2 \leftarrow 2$		983.66	−18.7	87.2	−0.4	2
$3 \leftarrow 2$	$0 \leftarrow -1$	$1 \leftarrow 3$		985.76	−37.7	66.3	2.3	2
$3 \leftarrow 3$	$1 \leftarrow 2$	$1 \leftarrow 1$		1089.01	27.0	93.0	−8.6	6
$1 \leftarrow 1$	$0 \leftarrow 1$	$3 \leftarrow 1$		1141.92	−18.1	75.5	3.0	2
$3 \leftarrow 2$	$2 \leftarrow 3$	$1 \leftarrow 1$		1144.71	−13.7	142.5	0.9	4
$3 \leftarrow 3$	$1 \leftarrow 0$	$1 \leftarrow 1$		1147.61	37.2	78.0	−0.4	2
$1 \leftarrow 2$	$2 \leftarrow 1$	$1 \leftarrow 1$		1156.79	11.5	158.5	−1.7	2
$3 \leftarrow 3$	$0 \leftarrow 1$	$1 \leftarrow 1$		1162.68	36.5	114.5	−2.5	2
$2 \leftarrow 2$	$0 \leftarrow -1$	$2 \leftarrow 2$		1382.34	17.4	90.3	−1.6	2
$4 \leftarrow 3$	$3 \leftarrow 4$	$1 \leftarrow 1$		1389.92	−26.6	80.2	4.8	8
$4 \leftarrow 4$	$1 \leftarrow 2$	$1 \leftarrow 1$		1482.33	37.3	80.2	−1.8	2
$2 \leftarrow 2$	$0 \leftarrow 1$	$2 \leftarrow 2$		1496.78	16.4	217.5	−3.2	2
$1 \leftarrow 2$	$2 \leftarrow 1$	$1 \leftarrow 1$		1519.41	−9.5	178.8	−0.2	2
$4 \leftarrow 4$	$1 \leftarrow 0$	$1 \leftarrow 1$		1523.10	43.2	59.3	−6.2	6
$4 \leftarrow 4$	$0 \leftarrow 1$	$1 \leftarrow 1$		1525.69	43.5	70.4	2.2	6
$2 \leftarrow 2$	$1 \leftarrow 0$	$2 \leftarrow 2$		1537.06	13.6	112.1	−2.6	2
$2 \leftarrow 2$	$0 \leftarrow 1$	$1 \leftarrow 1$		1633.25	−14.5	208.9	0.6	2
$1 \leftarrow 2$	$0 \leftarrow -1$	$3 \leftarrow 1$		1635.25	23.1	65.0	−4.0	4
$2 \leftarrow 2$	$-1 \leftarrow -2$	$1 \leftarrow 1$		1659.82	16.5	117.0	−3.5	4
$1 \leftarrow 0$	$1 \leftarrow 0$	$1 \leftarrow 1$		1853.02	−16.4	189.9	3.8	4
$5 \leftarrow 5$	$1 \leftarrow 2$	$1 \leftarrow 1$		1861.08	42.9	61.9	−11.3	0*
$2 \leftarrow 2$	$-1 \leftarrow 0$	$1 \leftarrow 1$		1922.51	14.9	283.4	0.6	4
$2 \leftarrow 2$	$1 \leftarrow 1$	$1 \leftarrow 1$	$1 \leftarrow 1$	792.09	15.6	354.0	−0.3	2
$2 \leftarrow 2$	$1 \leftarrow 1$	$2 \leftarrow 2$	$0 \leftarrow 0$	792.89	15.6	353.9	−1.6	2
$2 \leftarrow 2$	$1 \leftarrow 1$	$3 \leftarrow 3$	$-1 \leftarrow -1$	793.59	15.7	353.9	−1.2	2
$3 \leftarrow 3$	$2 \leftarrow 2$	$1 \leftarrow 1$	$1 \leftarrow 1$	1123.15	30.0	230.5	0.3	2
$3 \leftarrow 3$	$2 \leftarrow 2$	$1 \leftarrow 1$	$0 \leftarrow 0$	1123.65	30.0	230.4	0.8	2

Table 3. (*continued.*)

N	M_J	$Id\sharp^{\iota}$	M_I (^{14}N)	Field (mT)	Tuning rate (MHz/mT)	Intensity (arb. units)	Obs.–calc. (MHz)	Assigned uncertainty (MHz)
Laser frequency 2252.0542 GHz (133.120 μm) concluded								
3 ← 3	2 ← 2	2 ← 1	−1 ← −1	1124.15	30.0	230.3	2.7	2
3 ← 3	1 ← 1	1 ← 1	1 ← 1	1126.84	33.5	100.5	3.9	2
3 ← 3	1 ← 1	3 ← 2	0 ← 0	1127.34	33.5	100.5	0.5	2
3 ← 3	1 ← 1	3 ← 1	−1 ← −1	1127.74	33.5	100.5	1.0	2
4 ← 4	3 ← 3	1 ← 1	1 ← 1	1509.84	38.3	158.4	−0.1	2
4 ← 4	3 ← 3	1 ← 1	0 ← 0	1510.34	38.4	158.3	0.4	2
4 ← 4	3 ← 3	1 ← 1	−1 ← −1	1510.84	38.4	158.3	2.3	2
3 ← 2	−1 ← −1	2 ← 3	1 ← 1	1814.00	−22.2	97.0	1.1	2
3 ← 2	−1 ← −1	2 ← 3	0 ← 0	1814.70	−22.1	97.2	2.2	2
3 ← 2	−1 ← −1	2 ← 3	−1 ← −1	1815.40	−22.1	97.4	5.4	2
2 ← 1	1 ← 0	1 ← 3	1 ← 1	640.10	−30.9	193.9	1.0	2
2 ← 1	1 ← 0	1 ← 3	0 ← 0	640.60	−30.9	193.9	2.1	2
2 ← 1	1 ← 0	1 ← 3	−1 ← −1	641.00	−30.9	193.8	0.4	2
2 ← 1	1 ← 2	1 ← 1	1 ← 1	890.28	−14.6	193.1	−1.9	2
2 ← 1	1 ← 2	1 ← 1	0 ← 0	890.78	−14.6	193.1	−1.1	2
2 ← 1	1 ← 2	1 ← 1	−1 ← −1	891.28	−14.6	193.1	0.1	2
2 ← 2	0 ← 1	1 ← 1	1 ← 1	894.98	18.9	265.9	−1.6	2
2 ← 2	0 ← 1	2 ← 2	0 ← 0	895.58	18.9	265.8	−0.9	2
2 ← 2	0 ← 1	3 ← 3	−1 ← −1	896.18	18.9	265.8	1.2	2
Laser frequency 2314.1113 GHz (129.550 μm)								
3 ← 2	2 ← 2	3 ← 1		285.71	11.5	12.6	−1.1	4
3 ← 3	1 ← 1	3 ← 1		1 271.55	41.5	37.8	−8.7	$0^{\propto}$
3 ← 3	0 ← 0	3 ← 1		1271.55	47.1	36.1	13.8	$0^{\propto}$
3 ← 3	2 ← 2	3 ← 1		1758.10	−24.4	72.4	4.6	2
3 ← 3	1 ← 1	3 ← 1		1796.81	−35.3	79.2	8.4	4
4 ← 3	1 ← 1	3 ← 3		1904.85	−47.4	37.6	0.2	2
4 ← 3	2 ← 2	3 ← 3		1908.31	−46.6	36.4	−1.9	2
4 ← 3	3 ← 3	3 ← 2		1 940.09	−47.4	22.9	−4.8	6
3 ← 3	0 ← 0	3 ← 1		1941.56	−46.5	41.3	12.0	8
3 ← 3	1 ← 0	3 ← 1		1281.12	43.2	52.7	5.6	4
3 ← 3	2 ← 1	3 ← 1		1293.79	37.6	90.7	5.1	4
3 ← 2	2 ← 1	2 ← 1		1786.71	−15.3	53.9	2.1	4
4 ← 3	2 ← 1	3 ← 3		1886.93	−45.2	30.2	−1.1	2
4 ← 3	3 ← 2	3 ← 3		1888.61	−44.4	46.1	6.6	8
4 ← 3	4 ← 3	2 ← 2		1923.79	−46.3	44.3	−21.3	0*

Table 3. (*concluded.*)

N	M_J	$Id\sharp^{\iota}$	M_I (^{14}N)	Field (mT)	Tuning rate (MHz/mT)	Intensity (arb. units)	Obs.–calc. (MHz)	Assigned uncertainty (MHz)
Laser frequency 2314.1113 GHz (129.550 μm) concluded								
$4 \leftarrow 3$	$-1 \leftarrow 0$	$3 \leftarrow 3$		1926.35	−51.0	20.4	−1.5	6
$3 \leftarrow 3$	$1 \leftarrow 0$	$3 \leftarrow 1$		1932.35	−44.6	45.5	64.1	0*
$4 \leftarrow 3$	$-3 \leftarrow -3$	$2 \leftarrow 2$	$1 \leftarrow 1$	212.83	14.8	73.9	0.4	2
$4 \leftarrow 3$	$-3 \leftarrow -3$	$2 \leftarrow 2$	$0 \leftarrow 0$	213.53	14.8	74.0	−0.2	2
$4 \leftarrow 3$	$-3 \leftarrow -3$	$2 \leftarrow 2$	$-1 \leftarrow -1$	214.33	14.8	74.0	−1.6	2
$3 \leftarrow 3$	$3 \leftarrow 2$	$2 \leftarrow 1$	$1 \leftarrow 1$	1310.45	33.7	114.6	5.8	2
$3 \leftarrow 3$	$3 \leftarrow 2$	$2 \leftarrow 1$	$0 \leftarrow 0$	1310.95	33.7	114.6	4.1	2
$3 \leftarrow 3$	$3 \leftarrow 2$	$2 \leftarrow 1$	$-1 \leftarrow -1$	1311.33	33.7	114.5	7.9	2
$3 \leftarrow 3$	$3 \leftarrow 2$	$2 \leftarrow 1$	$1 \leftarrow 1$	1727.19	−21.2	295.9	−1.3	2
$3 \leftarrow 3$	$3 \leftarrow 2$	$4 \leftarrow 2$	$0 \leftarrow 0$	1727.79	−21.2	295.9	−1.0	2
$3 \leftarrow 3$	$3 \leftarrow 2$	$6 \leftarrow 3$	$-1 \leftarrow -1$	1728.39	−21.2	295.9	−0.7	2
$3 \leftarrow 3$	$2 \leftarrow 1$	$5 \leftarrow 1$	$1 \leftarrow 1$	1772.80	−31.5	153.3	−4.3	2
$3 \leftarrow 3^{\&}$	$2 \leftarrow 1^{\alpha}$	$2 \leftarrow 2^{\beta}$	$0 \leftarrow 0$	1773.21	−31.5	153.3	−2.9	2
$3 \leftarrow 3$	$2 \leftarrow 1$	$7 \leftarrow 3$	$-1 \leftarrow -1$	1773.61	−31.5	153.3	−3.7	2

$^{\iota}$ The $id\sharp$ labels the state with the indicated value of M_F, in order of increasing energy, for a given value for N, the vibrational quantum number. Note however, that N is often not a good quantum number because adjacent vibrational levels are mixed by the magnetic field (see text).

* Broad or weak resonance.

$^{\ni}$ Region of extremely broad and overlapping resonances, see Fig. 6 and text.

$^{\propto}$ Double line.

& For this transition J values rather than $id\sharp$ are used in the calculation.

$^{\alpha}$ J values.

$^{\beta}$ M_J values.

4. Analysis

Since the $\nu_5 = 1 \leftarrow 0$ vibrational transition of a linear molecule is analogous to a $K_a = 1 \leftarrow 0$ rotational transition of a bent molecule and since we had computer code available for an asymmetric rotor model, it was decided to use this program to analyze the spectra. By truncating the basis set to a single value of K_a, the asymmetric rotor treatment can be made equivalent to treating the transition as one involving two vibrational states. The parameters determined using the asymmetric rotor model are readily converted to those parameters appropriate to a linear molecule in its $\nu_5 = 0$ and 1 levels as shown in Table 2. Although numerous modifications to the code have occurred over the years, the basic computer program is described by Sears [21,22].

The asymmetric rotor Hamiltonian used in the analysis may be expressed as the sum of several terms [17,22]

$$\boldsymbol{H}_{\text{eff}} = \boldsymbol{H}_{\text{r}} + \boldsymbol{H}_{\text{cd}} + \boldsymbol{H}_{\text{ss}} + \boldsymbol{H}_{\text{sscd}} + \boldsymbol{H}_{\text{sr}} + \boldsymbol{H}_{\text{srcd}} + \boldsymbol{H}_{\text{sI}} + \boldsymbol{H}_{\text{Q}} + \boldsymbol{H}_{\text{Z}} \quad (1)$$

The details of the individual terms, $\boldsymbol{H}_{\text{r}}$, $\boldsymbol{H}_{\text{cd}}$, $\boldsymbol{H}_{\text{ss}}$, $\boldsymbol{H}_{\text{sr}}$, $\boldsymbol{H}_{\text{srcd}}$, $\boldsymbol{H}_{\text{sI}}$, $\boldsymbol{H}_{\text{Z}}$ are given in refs. 17, 22–27. A brief review of the various terms is given here.

$\boldsymbol{H}_{\text{r}}$ is the rigid rotor Hamiltonian given as

$$\boldsymbol{H}_{\text{r}} = AN_{\text{a}}^2 + BN_{\text{b}}^2 + CN_{\text{c}}^2 \quad (2)$$

where A, B, and C are the rotational constants and $\boldsymbol{N}$ is the rotational angular momentum operator in units of $h/2\pi$.

Centrifugal distortion is taken into account by the term $\boldsymbol{H}_{\rm cd}$. Although this molecule is sufficiently near a prolate symmetric rotor that the "S" reduced form of the Hamiltonian is more appropriate, the "A" reduced form is equivalent here because of the truncation in the calculation and the levels under consideration (no $K = 2$). Therefore, the "A" reduced form [23] is used and is given to sextic terms by

$$\boldsymbol{H}_{\rm cd} = -\Delta_N \boldsymbol{N}^4 - \Delta_{NK} \boldsymbol{N}^2 N_{\rm a}^2 - \Delta_K N_{\rm a}^4 - 2\delta_N \boldsymbol{N}^2 (N_{\rm b}^2 - N_{\rm c}^2) - \delta_K [N_{\rm a}^2, (N_{\rm b}^2 - N_{\rm c}^2)]_+$$

$$+ \Phi_N \boldsymbol{N}^6 + \Phi_{NK} \boldsymbol{N}^4 N_{\rm a}^2 + \Phi_{KN} \boldsymbol{N}^2 N_{\rm a}^4 + \Phi_K N_{\rm a}^6 + 2\phi_N \boldsymbol{N}^4 (N_{\rm b}^2 - N_{\rm c}^2)$$

$$+ \phi_{NK} \boldsymbol{N}^2 [N_{\rm a}^2, (N_{\rm b}^2 - N_{\rm c}^2)]_+ + \phi_K [N_{\rm a}^4, (N_{\rm b}^2 - N_{\rm c}^2)]_+ \quad (3)$$

Fine structure interactions are included by the terms $\boldsymbol{H}_{\rm ss}$ and $\boldsymbol{H}_{\rm sr}$. The spin–spin dipolar Hamiltonian accounts for the interaction between the two unpaired electrons and is given by [24]

$$\boldsymbol{H}_{\rm ss} = (D/3)[2S_{\rm a}^2 - S_{\rm b}^2 - S_{\rm c}^2] + E[S_{\rm b}^2 - S_{\rm c}^2] \quad (4)$$

where $D = 3\alpha$ and $E = \beta$.

$\boldsymbol{H}_{\rm sscd}$ accounts for the centrifugal distortion correction of the spin–spin interaction and is given by

$$\boldsymbol{H}_{\rm sscd} = 1/2 D\alpha_N [\boldsymbol{N}^2, (2S_{\rm a}^2 - S_{\rm b}^2 - S_{\rm c}^2)]_+ + 1/2 D\alpha_K [\boldsymbol{N}_{\rm a}^2, (2S_{\rm a}^2 - S_{\rm b}^2 - S_{\rm c}^2)]_+$$

$$+ 1/2 \Phi_{NK}^{\alpha} \boldsymbol{N}_{\rm a}^2 [\boldsymbol{N}^2, (2S_{\rm a}^2 - S_{\rm b}^2 - S_{\rm c}^2)]_+ \quad (5)$$

where $D\alpha_N$ and $D\alpha_K$ represent the rotational dependence and the K dependence of the centrifugal distortion for the spin–spin coupling, respectively.

The spin-rotation interaction Hamiltonian is given by

$$\boldsymbol{H}_{\rm sr} = \epsilon_{\rm aa} N_{\rm a} S_{\rm a} + \epsilon_{\rm bb} N_{\rm b} S_{\rm b} + \epsilon_{\rm cc} N_{\rm c} S_{\rm c} \quad (6)$$

and the centrifugal distortion effects on $\boldsymbol{H}_{\rm sr}$ to quartic terms by

$$\boldsymbol{H}_{\rm srcd} = \Delta_K^s N_{\rm a}^3 S_{\rm a} + \Delta_{KN}^s N_{\rm a}^2 \boldsymbol{N} \bullet \boldsymbol{S} + \frac{1}{2} \Delta_{NK}^s [\boldsymbol{N}^2, N_{\rm a} S_{\rm a}]_+ + 2\delta_N^s (N_{\rm b}^2 - N_{\rm c}^2)(\boldsymbol{N} \bullet \boldsymbol{S})$$

$$+ \delta_K^{\rm s} [(N_{\rm b}^2 - N_{\rm c}^2), N_{\rm a} S_{\rm a}]_+ \quad (7)$$

$\boldsymbol{H}_{\rm SI}$ represents the hyperfine magnetic interaction between the unpaired electron spins and the net nuclear spin and may be written in Cartesian representation [22] as

$$\boldsymbol{H}_{\rm SI} = a_{\rm FC} \boldsymbol{S} \bullet \boldsymbol{I} + \boldsymbol{S} \bullet \boldsymbol{T} \bullet \boldsymbol{I} \quad (8a)$$

where the first term represents the isotropic Fermi contact interaction and the second term represents the spin–spin dipole–dipole interaction energy. In this case, we write

$$\boldsymbol{H}_{\rm IS} = a_F (\boldsymbol{S} \bullet \boldsymbol{I}) + (aa)_I S_{\rm a} I_{\rm a} + (bb)_I S_{\rm b} I_{\rm b} + (cc)_I S_{\rm c} I_{\rm c} + (ab)_I (S_{\rm a} I_{\rm b} + S_{\rm b} I_{\rm a}) \quad (8b)$$

where $(aa)_I + (bb)_I + (cc)_I = 0$.

Table 4. Millimetre wave data {MHz} for the $\nu_5 = 0$ and 1 used in the fit of the present work.

	$J' \leftarrow J'$								
	$N'+1 \leftarrow N+1$			$N' \leftarrow N$			$N'-1 \leftarrow N-1$		
$N' \leftarrow N$	Frequency	Obs.–calc.[¶*]	Obs.–calc.[f]	Frequency	Obs.–calc.[¶*]	Obs.–calc.[f]	Frequency	Obs.–calc.[¶*]	Obs.–calc.[f]
$v_5 = 0$									
11 ← 10[¶]	217 890.591	0.004	–0.004	217 920.889	0.001	–0.000	217 957.123	–0.010	–0.005
13 ← 12[¶]	257 507.383	0.058	0.050	257 533.747	0.025	0.016	257 563.358	0.027	0.048
14 ← 13[¶]	277 313.451	–0.004	–0.017	277 338.433	–0.036	–0.049	277 365.849	0.008	0.029
15 ← 14[¶]	297 118.091	–0.005	–0.025	297 141.971	–0.013	–0.032	297 167.550	–0.027	–0.007
16 ← 15[¶]	316 921.209	–0.011	–0.038	316 944.189	0.009	–0.017	316 968.328	–0.005	0.012
18 ← 17[¶]	356 522.767	0.042	–0.002	356 544.291	0.027	–0.016	356 566.267	0.019	0.025
19 ← 18[¶]	376 320.961	–0.026	–0.080	376 341.962	–0.014	–0.067	376 363.119	–0.011	–0.013
8 ← 7	158 452.780	0.023	0.054	158 494.595	–0.005	–0.002	158 553.392	–0.013	–0.097
9 ← 8	178 267.390	0.022	0.040	178 304.174	–0.011	–0.007	178 352.608	0.017	–0.037
10 ← 9	198 079.896	0.031	0.039	198 112.983	0.004	0.009	198 154.287	0.016	–0.017
12 ← 11	237 699.709	–0.002	–0.007	237 727.855	0.011	0.018	237 760.300	0.013	0.009
13 ← 12	257 507.296	–0.030	–0.037	257 533.736	–0.004	0.004	257 563.353	0.038	0.043
14 ← 13	277 313.446	–0.012	–0.022	277 338.481	–0.013	–0.001	277 365.879	0.047	0.059
15 ← 14	297 118.106	0.002	–0.010	297 142.020	0.003	0.017	297 167.613	0.036	0.056
16 ← 15	316 21.184	–0.052	–0.063	316 944.177	–0.047	–0.029	316 968.273	–0.069	–0.043
17 ← 16	336 722.803	–0.003	–0.014	336 745.026	0.002	0.022	336 767.898	–0.061	–0.029
18 ← 17	356 522.738	–0.022	–0.031	356 544.314	–0.017	0.007	356 566.214	–0.066	–0.028
19 ← 18	376 321.098	0.065	0.057	376 342.145	0.087	0.116	376 363.234	0.057	0.102
$v_5 = \pm 1$									
8 ← 7	158 274.330	0.019	0.083	158 464.488	–0.008	–0.014	158 345.069	0.034	–0.063
	159 090.573	–0.002	0.051	159 267.073	0.057	0.055	159 133.398	–0.019	–0.099
9 ← 8	178 082.286	0.019	0.062	178 224.251	–0.055	–0.055	178 151.088	0.022	–0.036
	178 998.257	–0.014	0.018	179 129.917	0.070	0.071	179 046.048	–0.012	–0.057
10 ← 9	197 884.774	0.030	0.059	197 995.158	–0.056	–0.052	197 949.866	0.037	0.007
	198 900.692	–0.019	–0.002	199 003.061	0.074	0.078	198 949.440	–0.003	–0.025
12 ← 11	237 479.105	0.004	0.012	237 552.475	–0.092	–0.084	237 536.571	0.038	0.041
13 ← 12	257 272.492	0.037	0.037	257 334.661	–0.012	–0.004	257 326.699	0.079	0.092
	258 588.825	–0.054	–0.065	258 646.794	0.123	0.127	258 634.295	0.004	0.022

14←13	277 063.838	0.076	0.070	277 117.499	–0.040	–0.033	277 115.201	0.110	0.130
	278 480.272	–0.097	–0.114	278 530.520	0.075	0.079	278 524.342	–0.044	–0.021
15←14	296 853.242	0.035	0.023	296 900.402	–0.112	–0.107	296 902.142	0.049	0.074
	298 369.835	–0.126	–0.150	298 414.307	0.163	0.165	298 412.626	–0.054	–0.027
16←15	316 640.768	–0.124	–0.140						
	318 257.667	–0.069	–0.098	318 297.326	–0.007	–0.008	318 299.202	–0.075	–0.046
17←16	336 426.859	–0.003	–0.025	336 464.926	–0.184	–0.182	336 471.774	–0.063	–0.034
	338 143.676	–0.046	–0.079	338 179.796	0.102	0.099	338 184.082	–0.128	–0.099
18 ← 17	356 211.168	0.038	0.012	356 246.048	–0.104	–0.106	356 254.491	–0.048	–0.020
	358 027.982	0.068	0.030				358 067.495	0.029	0.058
19 ← 18	375 993.837	0.157	0.126	376 026.113	0.039	0.033	376 035.807	0.076	0.102
	377 910.350	0.067	0.023				377 949.018	0.013	0.039

[¶]Values and Observed – Calculated values from Brown et al. [11].

[*]Observed – calculated values from McCarthy et al. [14,28].

[f] Observed – calculated values from this work.

The Hamiltonian $\boldsymbol{H}_{\rm Q}$ accounts for the electric quadrupole interaction of the ^{14}N nucleus and is given in Cartesian form as

$$\boldsymbol{H}_{\rm Q} = \boldsymbol{I} \bullet \boldsymbol{Q} \bullet \boldsymbol{I} \tag{9a}$$

In this case,

$$\boldsymbol{H}_{\rm Q} = (aa)_{\rm Q} I_{\rm a}^2 + (bb)_{\rm Q} I_{\rm b}^2 + (cc)_{\rm Q} I_{\rm c}^2 + (ab)_{\rm Q}(I_{\rm a} I_{\rm b} + I_{\rm b} I_{\rm a}) \tag{9b}$$

and again $(aa)_{\rm Q} + (bb)_{\rm Q} + (cc)_{\rm Q} = 0$.

$\boldsymbol{H}_Z$ takes account of the interaction of the radical with the external magnetic field and is given by

$$\boldsymbol{H}_Z = \mu_{\rm B} \boldsymbol{B} \bullet \boldsymbol{g}_{\rm s} \bullet \boldsymbol{S} + \mu_{\rm N} \boldsymbol{B} \bullet \boldsymbol{g}_{\rm r} \bullet \boldsymbol{N} - g_I \mu_{\rm N} I_{\rm z} B \tag{10}$$

where $\boldsymbol{B}$ is the applied field, $\mu_{\rm B}$ is the Bohr magneton and $\mu_{\rm N}$ is the nuclear magneton. The first term accounts for the isotropic and anisotropic interactions of the electron spin with the field, while the second term accounts for the rotational Zeeman effect and the last term accounts for the nuclear spin Zeeman term. The isotropic part of the diamagnetic susceptibility does not affect the transition frequency and the effect of the anisotropic part is too small to be determined at these fields.

The effective Hamiltonian was used to analyze the data presented in Tables 3 and 4. Of the many parameters listed above only those needed for the zero field linear molecule Hamiltonian used by McCarthy et al. [14,28] plus the band origin, and the Zeeman and hyperfine structure parameters were used in fitting. Thus, A, B, C, Δ_N, Δ_{NK}, δ_N, Φ_{NK} from the rotational Hamiltonian, α, β, Δ_N^α, Δ_K^α, and Φ_{NK}^α from the spin–spin Hamiltonian, $\epsilon_{aa}, \epsilon_{bb}, \epsilon_{cc}, (\Delta_{NK}^S + \Delta_{KN}^S)$ from the spin–rotational Hamiltonian, a_F, $(aa)_I$, $1/2[(bb)_I - (cc)_I]$, $(aa)_{\rm Q}$, and $1/2[(bb)_{\rm Q} - (cc)_{\rm Q}]$ from the hyperfine Hamiltonian, and g_{aa}^s, $1/2(g_{bb}^s + g_{cc}^s)$, $1/2(g_{bb}^s - g_{cc}^s)$, $1/2(g_{bb}^r + g_{cc}^r)$, $1/2(g_{bb}^r - g_{cc}^r)$ from the Zeeman Hamiltonian were fitted. It was found that $1/2[(bb)_I - (cc)_I]$, $(aa)_{\rm Q}$, and $1/2[(bb)_{\rm Q} - (cc)_{\rm Q}]$ have larger uncertainties than their magnitudes and the fitting of the resonances with hyperfine structure was not appreciably improved by including any of these three constants. Therefore, they were fixed at the values found for HCCN.[3] Table 3 provides details on the laser line used to observe the resonance, the field of the resonance, the assignment of the line, the observed – calculated values for the frequency and field, the predicted tuning rate, the predicted intensity, and the uncertainty assigned to the observed field.

A comment is needed here about the assignment of the lines. As can be seen from Fig. 5, the Zeeman shifts are larger than the rotational spacing for low N and there are numerous avoided crossings. Often neither N nor J is even approximately a good quantum number. The analysis program recognizes that J may not be a good quantum number but assumes that N is good since most cases previously treated were of very light molecules with large rotational constants. Fortunately, when hyperfine structure was not present, no problems were encountered in assigning N and J values that the computer program could use to find the correct eigenvalues. However, this was not generally true when hyperfine structure was resolved. In this case, the identification of the correct eigenvalue presented a challenge. We fear that the N and J or level number quantum numbers listed are valid only in the context of this particular computer program and should not be given too great a physical significance. Indeed, the only rigorous way of assigning quantum numbers here is to order the eigenvalues for a particular M_F value in order of increasing energy and to identify a level by M_F and eigenvalue number. As an infinite matrix is being truncated, this would be quite tedious for high N .

In addition to the observed LMR resonances, millimeter wave data for $\nu_5 = 0$ from Brown et al. [11] and $\nu_5 = 0$ and 1 from McCarthy et al. [14,28] were used in the fit and are presented in Table 4. Table 4

[3] M.D. Allen, K.M. Evenson, and J.M. Brown. Manuscript in preparation.

Table 5. Molecular parameters determined in least-squares fit to observed microwave and LMR data for DCCN in the $v = 5$ level of the $X^3\Sigma^-$ state.*

Parameter	This work (MHz)
A	2253 633.45 (22)
$\frac{1}{2}(B + C)$	9 906.370 9 (15)
$\frac{1}{4}(B - C)$	25.313 9 (14)
D_N	0.003 6611 (27)
D_{NK}	−16.611 7 (20)
d_N	0.000 1533 (26)
Φ_{NK}	0.000 0981 (38)
α	9 046.29 (38)
β	740.74 (60)
D_N^α	0.010 04 (65)
D_K^α	−198.35 (42)
Φ_{KN}^α	−0.004 87 (95)
ϵ_{aa}	−2.65 (92)
$\frac{1}{2}(\epsilon_{bb} + \epsilon_{cc})$	−15.051 (16)
$\frac{1}{2}(\epsilon_{bb} - \epsilon_{cc})$	−0.541 (31)
$\Delta_{NK}^S + \Delta_{KN}^S$	0.416 (23)
Δ_{NK}^S	−0.71 (15)
a_F (N)	12.10 (42)
aa_I (N)	−10.82 (82)
bb_I (N)	7.46♯
aa_Q (N)	−1.9481♯
bb_Q (N)	0.974♯
g_s^{aa}	2.002 337 (48)&
$\frac{1}{2}(g_s^{bb} + g_s^{cc})$	2.003 047 (38)&
$\frac{1}{2}(g_s^{bb} - g_s^{cc})$	$-0.65(67) \times 10^{-4}$&
g_r^{aa}	0.0♯
$\frac{1}{2}(g_r^{bb} + g_r^{cc})$	$0.14(17) \times 10^{-4}$&
$\frac{1}{2}(g_r^{bb} - g_r^{cc})$	$-0.12(17) \times 10^{-3}$&

*Numbers in parentheses are one standard deviation and apply to the last quoted digits.
♯Parameter constrained to this value in the fit.
&Dimensionless quantities.

provides details of the microwave frequency, the assignment, and the observed–calculated values for Brown et al. [11] and McCarthy et al.'s [28] fits and the fit in this work.

The microwave transitions of Brown et al. [11] and McCarthy et al. [14,28] were given an uncertainty of 100 kHz in the fitting. Most of the LMR transitions were given an uncertainty of 2 MHz. As the tuning rates varied from 6 to slightly over 50 MHz/mT, the uncertainty assigned to the observed field varied from about 0.3 to 0.04 mT. The weighting scheme is rationalized to some extent by the idea that the widths of the resonances in field are inversely proportional to tuning rate. However, almost all of the lines contain unresolved hyperfine structure, which may make the line width more or less independent of tuning rate. A number of the LMR resonances were given larger uncertainties where the line shape

Table 6. Comparison of HCCN and DCCN ^{14}N hyperfine parameters (MHz).

Parameter	HCCN*	DCCN
a_F (N)	11.573 8 (19)	12.10 (42)
aa_l (N)	−18.853 5 (50)	−10.82 (82)
bb_l (N)	7.46 (21)	♯
$(aa)_Q$ (N)	−1.948 1 (34)	♯
$(bb)_Q$ (N)	0.974	♯
g_s^{aa}	2.002 238 (42)	2.002 339 (48)
$\frac{1}{2}(g_s^{bb} + g_s^{cc})$	2.002 785 (34)	2.003 047 (38)
$\frac{1}{2}(g_s^{bb} - g_s^{cc})$	0.0**	$-0.65(67) \times 10^{-4}$
$\frac{1}{2}(g_r^{bb} + g_r^{cc})$	0.0**	$0.15(17) \times 10^{-4}$
$\frac{1}{2}(g_r^{bb} - g_r^{cc})$	0.0**	$-0.13(17) \times 10^{-3}$

*M.D. Allen, K.M. Evenson, and J.M. Brown. Manuscript in preparation.

**Parameter constrained to this value in HCCN fit.

♯These values fixed at HCCN values.

Table 7. Comparison of linear parameters with previous work (MHz).&

Parameter	This work	McCarthy et al. [14]
ν_0 of ν_5 (GHz)	2 243.727 08 (21)	2 243.8 (6)*
B_0	9 906.370 9 (14)	9 906.370 8 (4)
$D_0 \times 10^3$	3.661 1 (27)	3.660 1 (7)
γ_0	− 15.051 (16)	−15.093 (8)
λ_0	13 569.4 (6)	13 602 (5)
$\lambda_{D0} \times 10^3$	15.1 (10)	15.3 (3)♯
B_1	9 922.982 6 (13)	9 922.983 5 (2)
$D_1 \times 10^3$	3.563 0 (26)	3.564 4 (4)
γ_1	−14.635 (17)	−14.705 (3)
λ_1	13 271.9 (5)	13 259.3 (9)
$\lambda_{D1} \times 10^3$	7.75 (98)	7.7 (2)
o	740.74 (53)	740.2 (8)
p	0.541 (31)	0.568 (9)
$q \times 10^3$	50.627 8 (28)	50.627 6(4)
$q_D \times 10^3$	−0.306 6 (52)	−0.306 7 (7)

&ν_0 value in GHz.

*Value from Sun et al. [16] 74.845(2) cm^{-1}.

♯Sign confirmed by M.C. McCarthy.

appeared distorted. The uncertainties are included in Table 3.

5. Discussion

Table 5 presents the molecular parameters determined in the least squares fit to the observed microwave and LMR data for DCCN in the $\nu = 5$ level of the X $^3\Sigma^-$ state.

In Table 6, the ^{14}N hyperfine coupling constants of DCCN are compared with the ^{14}N constants of

HCCN from Allen et al. [4]

Table 6 also compares the g_s^{aa} and $1/2(g_r^{bb} + g_r^{cc})$ values from this work with those from Allen et al. Generally, these constants are much better determined for HCCN. This is probably partly the result of many more lines where the hyperfine structure is completely resolved. The unresolved D hyperfine structure in the DCCN spectrum probably distorts the line shapes. Essentially there is more HCCN data with resolved hyperfine structure and it is completely resolved.

It is unfortunate that we are unable to determine the difference in ^{14}N coupling constants between HCCN and DCCN. It is expected that the hyperfine coupling constants will depend strongly upon HCC bond angle because the carbene resonance H—C̈—C≡N is favoured when the molecule is bent and the allene resonance form H—Ċ = C = Ṅ is favoured when the molecule is linear. These resonance structures should have rather different ^{14} N hyperfine coupling constants.

Table 7 presents a comparison of the linear constants calculated from this work with those obtained by McCarthy et al. [14]

The microwave spectra effectively determines all the zero field parameters except A (or ν_5), ϵ_{aa}, and the hyperfine coupling constants as can be seen by the good agreement with McCarthy et al's. [14,28] measurements in Table 4 and constants in Table 7. ν_5 is more precisely determined than it is by the mid-IR as also shown in Table 7. The LMR data do determine the magnetic hyperfine coupling constants a_F and $(aa)_I$ reasonably well, but the uncertainties in $\frac{1}{2}[(bb)_I - (cc)_I]$ and the nuclear quadrupole coupling constants are larger than the constants, and these constants were fixed at HCCN values in the final fitting. The electron spin g tensor is reasonably well determined by the LMR data but the rotational g tensor is at best poorly determined.

Acknowledgement

This work was supported by the National Science Foundation and by the Robert A. Welch Foundation.

References

1. R.A. Bernheim, R.J. Kempf, P.W. Humer, and P.S. Skell. J. Chem. Phys. **41**, 1156 (1964).
2. R.A. Bernheim, R.J. Kempf, J.V. Gramas, and P.S. Skell. J. Chem. Phys. **43**, 196 (1965).
3. R.A. Bernheim, R.J. Kempf, and E.F. Reichenbecher. J. Magn. Reson. **3**, 5 (1970).
4. E. Wasserman, W.A. Yager, and V.J. Kuck. Chem. Phys. Lett. **7**, 409 (1970).
5. A. Dendramis and G.E. Leroi. J. Chem. Phys. **66**, 4334 (1977).
6. S. Saito, Y. Endo, and E. Hirota. J. Chem. Phys. **80**, 1427 (1984).
7. K.S. Kim, H.F. Schaefer, L. Radom, J.A. Pople, and J.S. Binkley. J. Am. Chem. Soc. **105**, 4148 (1983).
8. J.E. Rice and H.F. Schaefer. J. Chem. Phys. **86**, 7051 (1987).
9. P. Malmquist, R. Lindh, B.O. Roos, and S. Ross. Theor. Chim. Acta. **73**, 155 (1988).
10. E.T. Seidl and H.F. Schaefer. J. Chem. Phys. **96**, 4449 (1992).
11. F.X. Brown, S. Saito, and S. Yamamoto. J. Mol. Spectrosc. **143**, 203 (1990).
12. C.L. Morter, S.K. Farhat, and R.F. Curl. Chem. Phys. Lett. **207**, 153 (1993).
13. C.E. Miller, W.C. Eckhoff, and R.F. Curl. J. Mol. Struct. **352/353**, 435 (1995).
14. M.C. McCarthy, C.A. Gottlieb, A.L. Cooksy, and P. Thaddeus. J. Chem Phys. **103**, 7779 (1995).
15. J. Han, P.Y. Hung, J. DeSain, W.E. Jones, and R.F. Curl. J. Mol. Spectrosc. **198**, 421 (1999).
16. F. Sun, A. Kosterev, G. Scott, V. Litosh, and R.F. Curl. J. Chem. Phys. **109**, 8851 (1998).
17. T.J. Sears, P.R. Bunker, A.R.W. McKellar, K.M. Evenson, D.A. Jennings, and J.M. Brown. J. Chem. Phys. **77**, 5348 (1982).
18. R.J. Saykally, K.G. Lubic, A. Scalabrin, and K.M. Evenson. J. Chem. Phys. **77**, 58 (1982).
19. J.M. Brown, L.R. Zinck, and K.M. Evenson. Phys. Rev. A: At. Mol. Opt. Phys. **57**, 2507 (1998).

[4] M.D. Allen, K.M. Evenson, and J.M. Brown. Manuscript in preparation.

20. N.G. Douglas. Millimetre and submillimetre wavelength lasers. Springer Series in Optical Sciences. Vol. 61. Springer-Verlag Berlin, Heidelberg. 1989.
21. T.J. Sears. Comp. Phys. Commun. **34**, 123 (1984).
22. T.J. Sears. Comp. Phys. Rep. **2**, 1 (1984).
23. J.H. Van Vleck. Rev. Mod. Phys. **23**, 213 (1951).
24. J.K.G. Watson. *In* Vibrational spectra and structure. Vol. 6. *Edited by* J.R. Durig. Elsevier, New York. 1977. p. 1.
25. W.T. Raynes. J. Chem. Phys. **41**, 3020 (1964).
26. L.C. Bowater, J.M. Brown, and A. Carrington. Proc. R. Soc. London, Ser. A, **333**, 265 (1973).
27. J.M. Brown and T.J. Sears. J. Mol. Spectrosc. **75**, 111 (1979).
28. M.C. McCarthy, C.A. Gottlieb, A.L. Cooksy, and P. Thaddeus. AIP document No. PAPS 103-7779-15. Order by PAPS number and journal reference from American Institute of Physics, Woodbury, N.Y., 11797-2999, U.S.A.